12th International Conference on Fracture Mechanics of Concrete and Concrete Structures
FraMCoS-12
B.L.A. Pichler, Ch. Hellmich, P. Preinstorfer (Eds)

https://doi.org/10.21012/FC12.1131
TT-F:4

FRACTURE PROPAGATION OF CONCRETE AND ULTRA-HIGH-PERFORMANCE CONCRETE (UHPC) INTERFACE AFFECTED BY REPAIRED LAYER THICKNESS

ELHAM MAHMOUD[*] AND TOMOHIRO MIKI[†]

[*] Kobe University, Department of Civil Engineering
1-1 Rokkodai, Nada, Kobe, Japan
e-mail: 215t751t@stu.kobe-u.ac.jp

[†] Kobe University, Department of Civil Engineering
1-1 Rokkodai, Nada, Kobe, Japan
e-mail: mikitomo@port.kobe-u.ac.jp

Key words: UHPC Overlay, Reinforced concrete beams, Interface cracks between UHPC and NC.

Abstract: An integrated experimental and numerical study was conducted to understand the behavior of reinforced concrete (RC) wide beams with top UHPC overlay under a four-point bending load. An experimental study was carried out to assess the influence of different overlay thicknesses. It showed improvement in the structural performance compared with the beam without repair. In the numerical simulation, a three-dimensional finite element modeling was carried out, and its results were matched with the experimental results. This paper focuses on crack growth and stress around cracks at the interface between normal concrete and UHPC overlay. The FEM results showed that the locations of debonding occur at the pure moment zone, and delamination at the interface is caused by different stresses acting at the same location. At the interface surface where compression stress from the RC acts, tension stress from the UHPC overlay is also applied at the same location. Additionally, with a thinner overlay, partial delamination occurred at the interface because of the bending experienced throughout the repaired beam. Conversely, a 50 mm UHPC overlay provides sufficient stiffness to resist bending, which can lead to faster delamination over a larger area of the beam's surface.

1 INTRODUCTION

Heavy mechanical loads and severe weather conditions significantly affect the performance and durability of existing concrete structures. Structures like bridges are essential for urban life worldwide. When traffic loads are increased, the deck slab is subjected to higher mechanical loading, while the load-carrying capacity has to be enhanced accordingly. Rehabilitation and repair of structures and protection against chloride penetration and water ingress have increased. However, it must remain within the dead load weight of the structure to avoid necessitating strengthening interventions on other structural elements and the foundation.

One potential alternative material is Ultra-High-Performance Concrete (UHPC), known in Europe as Ultra-High-Performance Fiber Reinforced Concrete (UHPFRC). UHPC is a specialized cementitious material. It is defined as a cementitious composite material composed of an optimized gradation of granular constituents, a water-cementitious materials ratio of less than 0.25, and a high percentage of discontinuous internal fiber reinforcement. Its compressive strength is more significant than 150 MPa, and sustained post-cracking tensile strength is greater than 5 MPa. It has a discontinuous pore that reduces liquid ingress. [1] Steel fibers are incorporated into the UHPC

mixture at a volume of 1-3% [2]. These fibers enhance the UHPC's performance by improving crack resistance and increasing tensile strength [3]. It has shown high bond strength and good adherence to substrate material.

The first UHPC road bridge was designed and constructed in France in 2001 [4]. Switzerland was the first country to use Ultra-High-Performance Fiber Reinforced Concrete (UHPFRC) for rehabilitating a bridge deck in 2004, involving a span of 10 meters [5]. The first application of UHPC as a bridge deck overlay in the United States took place in May 2016 on a reinforced concrete slab bridge in Brandon, Iowa [6]. However, no established codes or standards clearly define UHPC; only technical guidelines and recommendations exist in certain countries, including Japan, the United States, and France.

The bond strength of the overlay substrate must be tested to ensure no interface failure between the existing concrete and the UHPC. Numerous experimental studies have been conducted to determine the interface shear bond stress using various methods, including direct tensile tests, splitting tensile tests, and slant shear tests. These studies have examined different variables, such as interface roughness, curing conditions, and substrate strength. However, no unified prediction model exists for the NC and UHPC interface. Experimental and analytical investigations have been conducted to understand the behavior of composite structural elements consisting of normal concrete and UHPC overlay.

The experimental study aimed to investigate the flexural behavior of reinforced concrete (RC) slabs and beams using a top-layer repair with UHPC. The experimental parameters included overlay thicknesses of 20 mm and 50 mm. The dimensions of the RC beams were 1500 x 400 x 200 mm, and no reinforcing steel was used at the overlay. The UHPC utilized a steel fiber content of 3% by volume. Four-point bending tests were conducted to determine failure modes, cracking patterns, and load-deflection characteristics.

Based on an experimental study, a 3D finite element model (FEM) analytical was developed for the prediction of the bending structural response of composite elements. The experimental and analytical study results will serve as a reference for designing bridge decks with UHPC overlay to enhance the bridge structures' service life.

The present study employs FEM to investigate the mechanisms of cracking diffusion in concrete repair systems. It aims to provide insights into cracking initiation, crack growth, overlay delamination, and propagation in a composite section of the wide beams repaired with top UHPC overlay under bending test.

2 EXPERIMENTAL PROGRAMS

The simple support beam tests were conducted under four-point bending conditions on wide beams that had been repaired with UHPC. The cross-sectional designs and reinforcement details of the specimens are illustrated in **Figure 1**. Each specimen has a total length of 1500 mm and a bending span of 1250 mm. The cross-section of the beam measures 200 mm in total depth, 400 mm in width, and 150 mm in effective depth, with a shear span of 550 mm. Two thicknesses were used for the top-repaired UHPC layer: 20 mm (WU-20) and 50 mm (WU-50), respectively. The reinforcement consists of three D13 steel bars with a yielding strength of 370 MPa on the tension side and two D06 bars on the compression side. The distance between the two concentrated loads applied to the beam was 150 mm.

2.1 Materials

Ordinary concrete comprises ordinary Portland cement, coarse aggregates, and fine

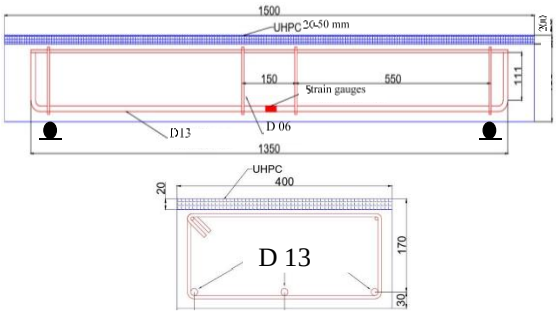

Figure 1: Wide RC beam dimensions (in mm)

Table 1: Material properties

Properties	NC	UHPC
Compressive strength (MPa)	41	117.3
Modulus of elasticity (GPa)	33	49.5
Tensile strength (MPa)	2.9	11.1

sand. UHPC includes ordinary Portland cement, fine sand, 3% steel fibers, and a water-reducing agent. The mechanical properties of both concrete and UHPC are presented in **Table** 1.

2.2. Test preparation

The RC beams were cast in a steel mold, and after two weeks, an UHPC layer was cast on top of the RC beams. The beams were kept at room temperature in the laboratory for one week before testing. For the good adhesion condition (noted as G), the beam interface was wet before the overlay was applied. During the testing, the structural behavior of the beams was observed and monitored by recording the applied loads, vertical displacements, and strain changes in the UHPC layer.

The load was applied using a control machine, which increased until failure occurred. Vertical displacements were measured using two displacement transducers positioned at the middle span for maximum displacement and at both supports to evaluate displacements in the opposite direction.

One strain gauge was installed at the top mid-span of the UHPC, while two were placed on the side of the beam at the repaired layer.

3 NUMERICAL SIMULATIONS

Our previous numerical study conducted a finite element model for the slant shear test. The developed finite element model (FEM) was designed to simulate the interface between normal concrete (NC) and UHPC to understand its behavior. The interface is subjected to shear and compressive stresses during the slant shear test. The failure mode observed in the slant shear was fracture mode II, while for RC beams with top UHPC overlay subjected to bending, the observed opening mode was mode I fracture.

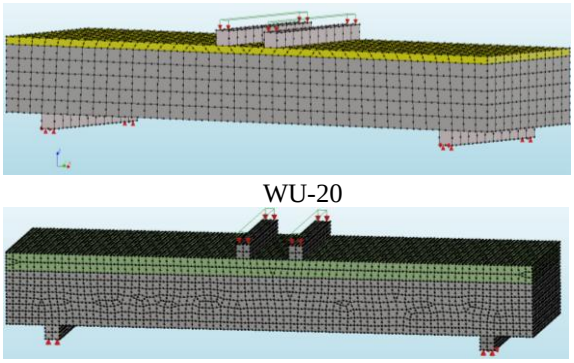

Figure 2 FE discretization with boundary conditions

The RC beams were subjected to a four-point bending test. Model analysis was conducted using the nonlinear FEM software, Diana version 10.6. **Figure 2** shows the beam discretization with boundary conditions.

The NC and UHPC were modeled using a total strain-based crack model. The tensile behavior was described with a smeared crack model. Both the NC and UHPC models utilized a parabolic model for compressive strength (f'_c) and an exponential model for tensile strength (f_t), as illustrated in **Figures 3(a)** and **(b)**, respectively. Nonlinear material properties of the steel reinforcement were defined according to the Von Mises criteria, as shown in **Figure 3(c)**. The steel plates were modeled using an elastic isotropic law, with an elastic modulus (E_s) of 200 GPa and a Poisson's ratio (v) of 0.3.

The boundary conditions for the supports were roller and hinged. The load was applied as a displacement control step. The Regular Newton-Raphson iterative method was used to calculate the structural response. 3D solid quadrilateral elements with eight nodes were used for NC and UHPC. The 3D simulation used a mesh size of 20 mm, as previously depicted in **Figure 2**. Steel reinforcement was embedded within the concrete. In contrast, no reinforcement was implemented at the UHPC-NC interface.

3D model was chosen for the wide beam due to the expected different stress distribution along the beam's width. FE modeling analyzes good adhesion condition (noted as G) parameters, as shown in **Table 2**. In the finite

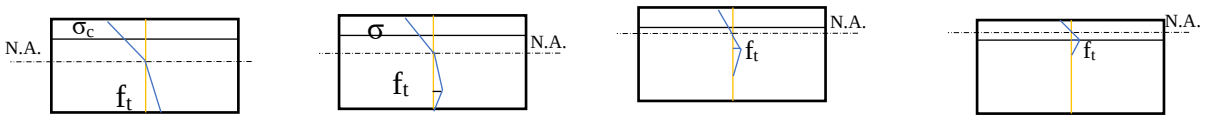

a) At the first crack where, the stress reached NC tensile strength.

b) At crack proportion, where the stress at the crack equals zero.

c) At interface delamination.

Figure 4: Crack development stages

element method (FEM), both normal and shear stresses at the interface were considered. The main parameters were K_n and K_s, representing the normal and shear stiffness moduli, respectively. The normal stiffness modulus, Kn, corresponds to the initial compressive stiffness of NC. Meanwhile, the shear stiffness modulus, Ks, is the initial slope of the shear stress-slip relationship. It changes based on interface surface conditions. It has a wide value range that should align with laboratory results.

Interface delamination primarily follows a linear and elastic behavior until separation occurs, at which point the initial shear stiffness reduces to zero, as shown in **Figure 3(d)**.

Additionally, the cohesion and the friction angle are considered, with specific values set to determine when delamination started. The interface shear stress was evaluated by Eq. (1).

$$\tau = C + \mu\, \sigma_n = C + \sigma_n \tan \phi \qquad (1)$$

where τ is the peak shear stress, C is the cohesion stress, μ is the coefficient of friction, and σ_n is stress normal to the shear plane.

Based on Eq. (1), the type of interface model indicates that the normal stress at the interface affects the shear strength. This interaction can lead to interface separation due to tensile stress acting in a normal direction to the shear plane. The finite element model of the beam demonstrated mode I fracture propagation at the interface between NC and UHPC overlay, which was consistent with experimental observations. The cracking processes in NC, UHPC, and at the interface plane can be influenced by various factors, including material properties, cohesion stress, and shear stiffness. The delamination is represented in this paper as an interface opening displacement equal to 0.1 mm. The model has been expanded to analyze the interface shear and normal stress.

Table 2: FEM parameters for 3D wide

NC	E_c 33000 MPa, ν 0.15, f'_c 40 MPa, f_t 2.9 MPa, G_F 0.09 N/mm.		
UHPC	E_{UHPC} 45000 MPa, ν 0.15, f'_c 117 MPa, f_t 11 MPa, G_F 20 N/mm.		
Reinforcing bar (tension)	E_s 200000 MPa, f_y 370 MPa, f_{ult}. 530 MPa		
Interface (NC/UHPC)	K_n 33000 N/ mm^3		
	Nonlinear elastic friction	K_s Min.	**G** 10
		C (MPa)	1.5
		ϕ (°)	60

As well as the effect of overlay thickness on interface delamination between NC and UHPC.

3.1 FEM Crack propagation

The stress is formulated in terms of relative displacement instated of strains at tensile behavior of concrete, UHPC, using a smeared crack model. Bazant and Oh eliminated the mesh dependency using a crack band model with constant fracture energy Gf [7]. The crack width w is related to the strain ε perpendicular to the crack with element length l, where $l = \sqrt{A}$, and A area of the element.

$$w = l\, \varepsilon \qquad (2)$$

Hillerborg et al. crack model assumed that fracture energy $G_f = \int_0^{w1} \sigma c\, dw$, σc crack band stress, w_1 crack width with zero stress [7]. microcrack width from zero to w1 is called process zone, and after that called macro cracks. Before cracking, the stress-crack width relation is assumed to be linear elastic material behavior.

It is assumed that a crack will propagate when the stress within an element reaches the tensile strength of the concrete, as shown in **Figure 4a**. Once the crack opens, the stress decreases with increasing crack width until it

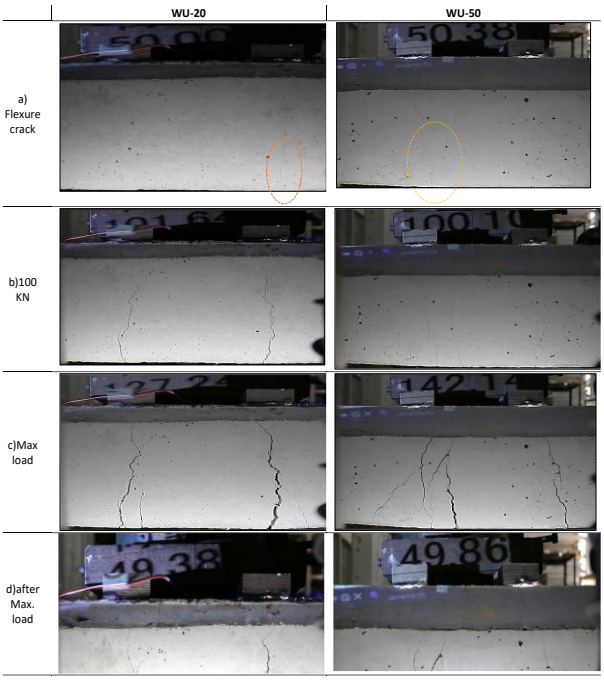

Figure 5: WU-20 and WU-50 experimental cracks at different loading stages.

ultimately reaches zero. A linear tension softening curve is applied to the stress-crack width curve. As the applied load increases, the crack opens and propagates, as illustrated in **Figure 4b**, while Figure 4c shows interface delamination. William et al. discussed fixed and rotating crack approaches for smeared cracks [8].

At fixed cracks, the crack system does not correspond to the principal strain if the direction of the loading changes. However, in the rotating crack model, the crack rotates with the principal strain. Our model is a rotating one. The bond between NC-UHPC is crucial for the composite material to transfer loads between the two materials effectively.

In this context, the interaction at the interface is represented by shear stress, which arises from mechanical interlock shear stiffness modulus Ks, cohesion stress, and friction angle. The development of bond stresses results from relative displacement between NC and UHPC.

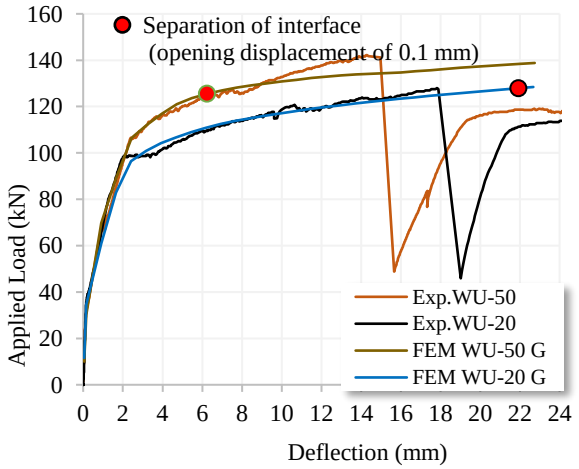

Figure 6: Test and FEM load – deflection WU-20/ 50

4 RESULTS AND DISCUSSION

4.1 Experimental results

The repaired beams WU-20 and WU-50 were tested under flexural load till bending failure occurred. Delamination at the interface was observed as bending cracks propagated through the NC-UHPC interface at the ultimate state. The failure mode of the beam specimens was flexural, characterized by the yielding of the reinforcing steel.

Figure 5 illustrates the crack propagation and compression in WU-20 and WU-50 with UHPC overlay at different loading stages. The cracks in the WU-50 were significantly finer compared to those in the WU-20 beam, up to 80% of the peak load. The bending cracks were initiated at the bottom surface edge of the beam, where the tension fiber is located.

As the load increased, the cracks propagated toward the upper edge of the beam till it reached NC- UHPC interface, as shown in **Figure 4c, Figure 5(c)**, **and (d),** which spread horizontally at the interface plane.

The cracks were widely opened at post-peak loading until failure. Both of the top repaired RC-wide beams with UHPC overlays WU-20 and WU-50, a loud sound was heard as the load reached its maximum. Separation at the interface was observed, and the UHPC overlay shifted horizontally.

Figure 6 illustrates the flexural load-deflection response of WU-20 and WU-50 across several phases. The first phase was a linear elastic phase. The second phase corresponded to the cracking, where the bending cracks started but the longitudinal reinforcing steel did not yield.

The next phase is the yielding of longitudinal

reinforcing steel. Then the peak phase, where the load increases to peak load. Followed by the failure phase with a rapid decrease of load with an increase in deflection.

WU-20 beam, flexural cracks were initiated at an applied load of 35 kN. These cracks were vertical and located at the bottom middle span of the beam.

As the load increased, flexural cracks propagated in the pure bending zone. Upon reaching the yield point, the cracks extended to the NC and UHPC overlay interface. From the yielding stage to the peak load, horizontal cracks were developed, and the strain gauges positioned between the NC and UHPC detected the delamination, as illustrated in **Figure 7(b)**.

Ultimately, during the post-peak failure loading stage, compressive cracks formed beneath the loading plates, leading to the crushing of the concrete.

In the case of WU-50, the initial bending cracks were observed at midspan when the load reached 30 kN. Then yielding of the longitudinal reinforcing steel occurred. As the applied load increases, the neutral axis shifts upward toward the compressive edge of the RC beam. The separation became visible, and a loud sound was heard at the peak load of 142.1 kN, accompanied by a midspan deflection of 15 mm, as indicated by the strain measurements captured by the strain gauges at the interface (see **Figure 7(a)**). The final phase is characterized by failure, which involves a rapid decrease in load.

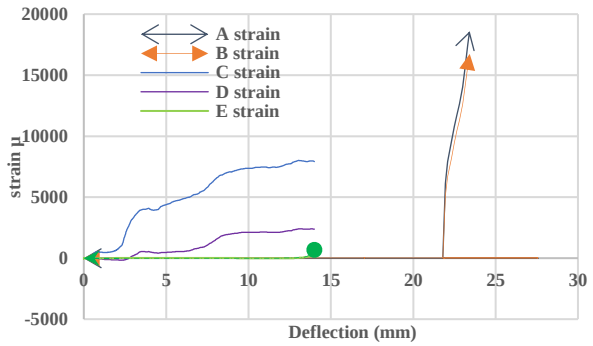

(a)WU-50

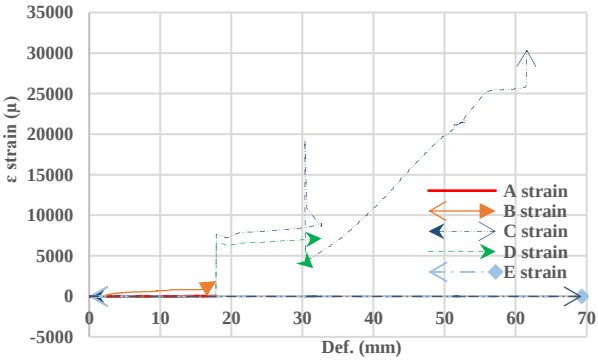

(b)WU-20

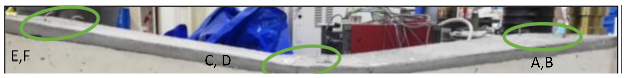

Figure 7: NC-UHPC interface strain deflection.

4.1 Numerical results

Figure 8(a) for WU-20G and **Figure 9(a)** for WU-50G present FEM analysis for the initial bending cracks that occurred at the middle bottom tension edge of the beam. The analysis showed that the tensile stress in the NC element exceeded its tensile capacity at [0.15 mm, 34 kN] and [0.15 mm, 30 kN] for WU 20-50, respectively.

Since NC and the UHPC are two distinct materials with different mechanical properties and were cased at different times, their behaviors under varying conditions of crack formation differed significantly.

Figure 8(b) for WU-20G and **Figure 9(b)** for WU-50G demonstrate that as the load increases, cracks develop vertically towards the compression beam fiber. When the tensile stress in the UHPC layer exceeds its tensile capacity, initial cracks form at the bottom surface of the UHPC overlay. The cracks initially appeared partially, and then a complete line under the loading plates became apparent.

At this stage, the displacement load was [0.9 mm, 73 kN] and [0.16 mm, 93 kN] for WU-20/50, respectively. It is important to note that, at this loading step, the delamination or interface opening gap in the Z direction had not yet reached 0.1mm, as shown in **Figure 8(c)** and **Figure 9(c)** for WU20/50, respectively. It can be observed that the WU-20 interface opening gap maximum movement was at four edges under loading points, while Wu-50 was wider at the pure bending zone. **Figure 8(d)** presents the stress distribution at the UHPC overlay; it shows that the maximum tensile stress for WU-20 was 16.78 MPa just under the

loading plates. While WU-50 max. tensile stress was 15 MPa at the pure bending zone, as shown in **Figure 9(d).**

At a yielding [3.0 mm, 102 kN] for WU20 and [3.2 mm, 113 kN] for WU50, cracks in the UHPC layer expanded horizontally beneath the area under the loading plates in the pure bending zone, as illustrated in **Figure 9(e)** for WU-50, while WU-20 shows that cracks are widespread just under the loading plates, as shown in **Figure 9(e). Figure 8(f)** shows cracks at [17.3 mm, 125.3 kN] for WU20, while **Figure 9(f)** displays cracks at [6.7 mm, 126 kN] for WU50. The interface delamination reached 0.1 mm, as shown in **Figure 8(l)** and **Figure 9(l)** for WU-20 and WU-50, respectively. **Figure 8(g)** presents the stress at the UHPC overlay for WU-20G. The max. tensile stress was 58.8 MPa, while the max. tensile stress for WU-50 was 15.6 MPa, as shown in **Figure 9(g)**.

It was observed that cracks on UHPC overlay to WU-20 were limited and at higher tensile stress as shown in **Figure 8(f)** and **(g)** compared with WU-50 in **Figure 9(f)** and **(g)**. That indicated that increasing the overlay thickness leads to wider interface separation and less tensile stress.

4.2 Comparison between the experimental and numerical results

The FEM analysis results for WU-50 indicate that during delamination, the stress in the bottom UHPC overlay under the loading plate area exceeds the UHPC tensile stress. Consequently, both the reinforced concrete (RC) and UHPC surfaces beneath the loading plates are filled with cracks in **Figure 9(g)**, which facilitates interface delamination in that region, similar to what was observed in the experimental study.

In contrast, for WU-20, at the delamination stage, the stress in the bottom UHPC overlay exceeds the UHPC tensile stress only under the loading plates (**Figure 8(g)**. In the experimental study, interface delamination occurred on one side of the beam, while the other side remained bonded. This behavior helps explain the interface strain-deflection response for WU-50

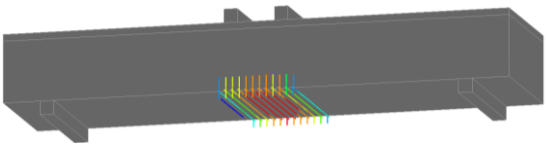

a) Isometric for 1st bending cracking of RC beam [0.15mm,34 KN].

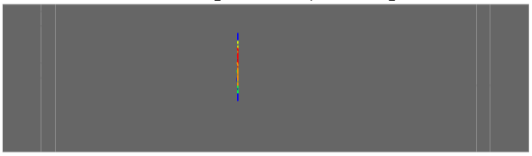

b) Cracks at UHPC bottom face at1st UHPC bending cracking [0.9mm,73KN]

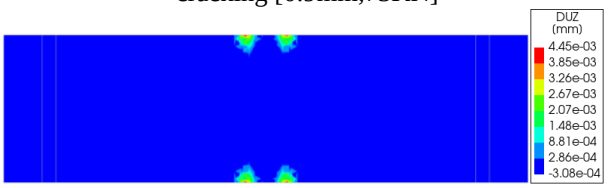

c) Interface opening distribution at1st UHPC bending cracking.

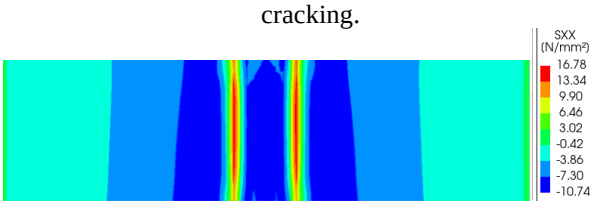

d) stress distrbution for UHPC bottom face at1st UHPC bending cracking.

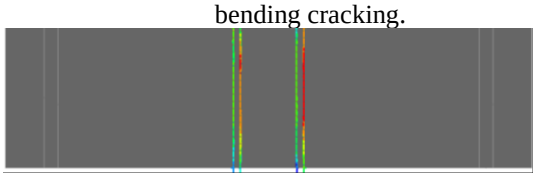

e) Cracks at UHPC bottom face at yielding [3.0 mm,102 KN].

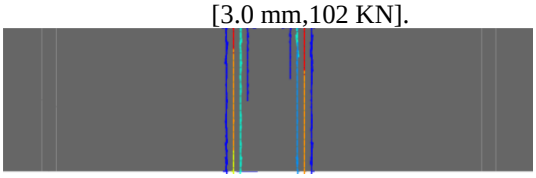

f) Cracks at UHPC bottom face at delamination [17.3mm,125.3 KN].

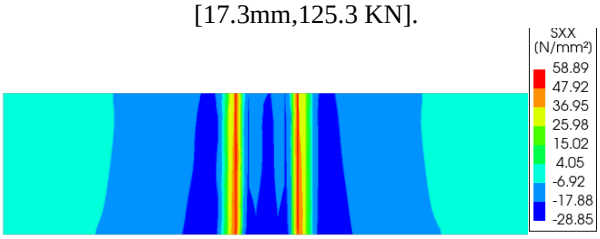

g) stress distribution of UHPC bottom face at delamination

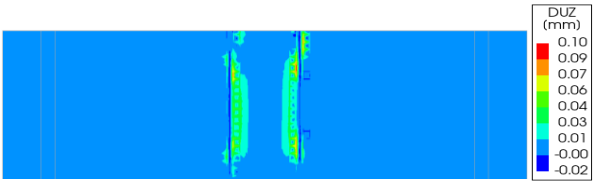

l) Interface opening distribution at delamination

Figure 8: Analytical results of WU-20G

and WU-20 experimental results, as illustrated in **Figure 7 (a)** and **(b)**, respectively. For WU-50, a significant sound of interface delamination was heard from the four strain gauges positioned along the interface. The strain gauge located in the middle recorded big movement, while the other strain gauges had no reading but at peak load were out. This indicates that the interface delamination started in the middle first at the maximum bending moment. **Figure 7(b)** for WU-20 indicates that the movement of the interface strain gauges was small compared to WU-50. However, this movement occurred at the middle span of the beam, and eventually, one of the edge strain gauges began to follow the movement of the middle gauge. It can be observed that when the overlays are thinner, interface delamination occurs partially due to bending across the entire beam section. In contrast, with a 50 mm UHPC overlay, the stiffness of the overlay is sufficient to prevent significant bending, leading to rapid delamination over a large area of the beam surface.

4.3 Crack patterns

Figure 10 and **11** compare the crack patterns observed in the experiments for W U-20 and WU-50 with those predicted by the finite element method (FEM). The results indicate that, at similar locations in the pure bending zone, the main cracks show an increase in width as the loading increases. **Figure 11** for WU-50 shows fine cracks compared with Wu-20 **Figure 10** at the same load value (yielding), the maximum crack width was 0.71mm for WU-50 while was 1.41 mm for WU-20. At peak load, the crack width was 2.61 mm for WU-50, while for WU-20, the maximum crack width was 6.31 mm.

4.4 Stress distribution

Figure 12 presents the finite element (FE) analysis results for the NC beam with a top UHPC overlay, specifically highlighting the stress distribution for WU 20 before any interface delamination occurs. The analysis reveals a significant difference in the stresses experienced by the NC and the UHPC overlay

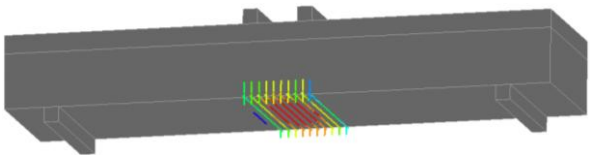

a) Isometric for 1st bending cracking of RC beam [0.15mm,30 KN].

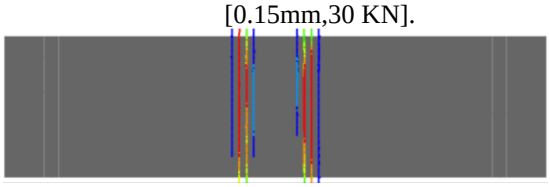

b) Cracks at UHPC bottom face at1st UHPC bending cracking [1.7mm, 93KN]

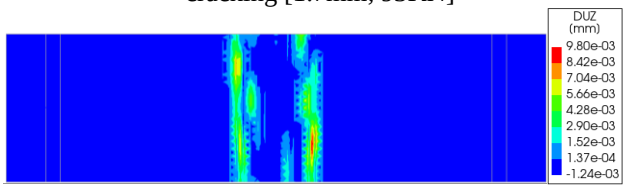

c) Interface opening distribution at 1st UHPC bending cracking.

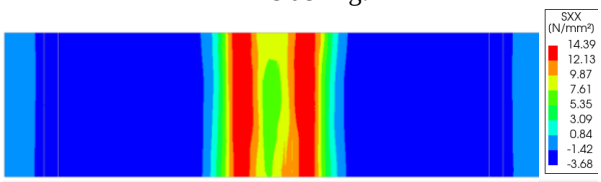

d) stress distrbution for UHPC bottom face at1st UHPC bending cracking.

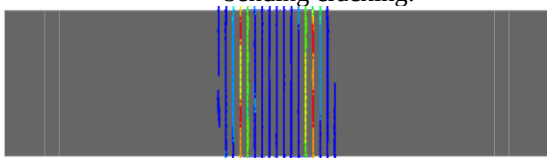

e) Cracks at UHPC bottom face at yielding [3.2mm,113KN].

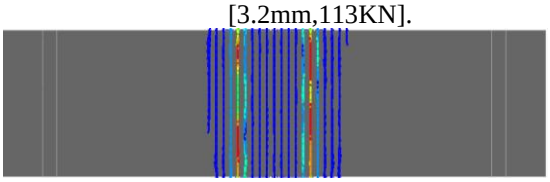

f) Cracks at UHPC bottom face at delamination [6.7mm,126KN].

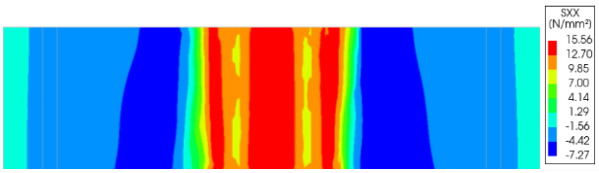

g) stress distribution of UHPC bottom face at delamination

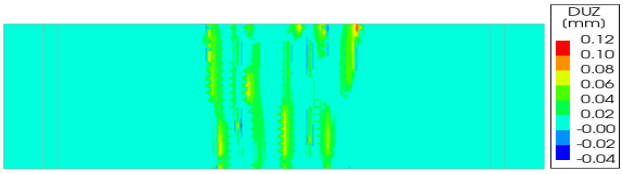

l) Interface opening distribution at delamination

Figure 9: Analytical results of WU-50G

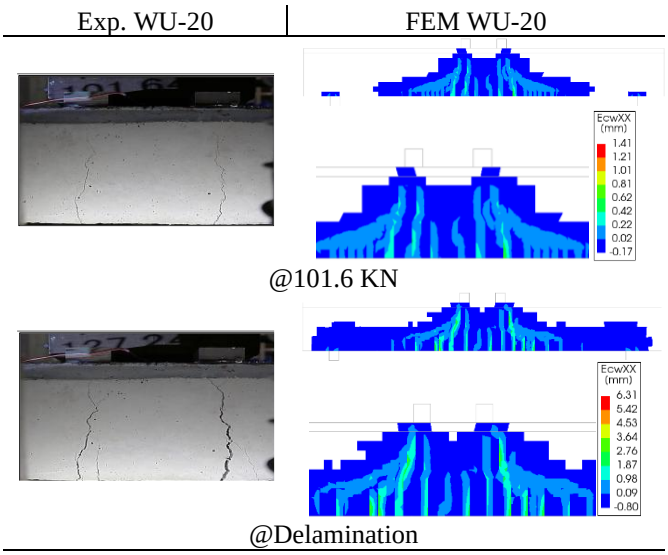

Figure 10: WU-20 Experimental & FEM cracks pattern

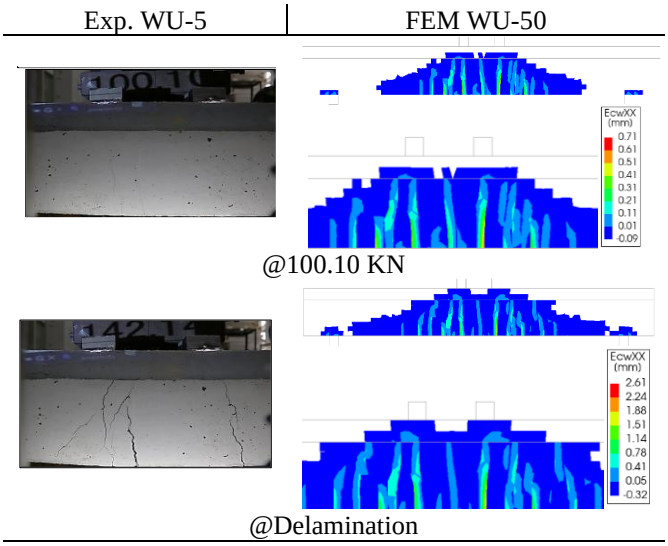

Figure 11: WU-50 Experimental & FEM cracks pattern

at the interface when subjected to bending loads. In **Figure 12(a)**, cracks can be observed in the composite section just before the UHPC bottom edge begins to crack. **Figure 12(b)** illustrates that the top edge of the reinforced concrete (RC) is under compression stress, reaching a maximum compressive stress of 15.8 MPa. Meanwhile, the UHPC overlay at the bottom edge is under tension, with a maximum tensile stress of 3.16 MPa. The tensile stress experienced by the NC is measured at 2.9 MPa. **Figure 12(c)** shows the cracking distribution just at the UHPC cracked, while **Figure 12(d)** indicates that the maximum tensile stress at the UHPC bottom edge reaches 16.78 MPa, whereas the RC stress remains in compression with low values.

FEM results for WU20 and WU-50 showed that before the top RC compression edge was cracked, the lower face of the UHPC overlay was in tension. That explains one of the reasons for interface delamination/cracking, which is caused by differing stresses at the same point.

5 CONCLUSIONS

The primary purpose of interface fracture mechanics is to define and assess the fracture energy release rate of interfaces and quantify fracture criteria for predicting crack paths. This paper introduces a finite element analysis of the stress distribution around cracks at the interface between two different materials based on an experimental study of top-repaired beams conducted at Kobe University.

One of the reasons for interface delamination occurs due to varying stress concentrations at the same point in the pure bending area. At one point, there was compression stress from the reinforced concrete (RC) and tension stress from the UHPC overlay. In normal concrete (NC), after cracking occurs, the stress drops to zero; however, in the UHPC layer, tensile stress persists even after cracking due to the use of steel fibers in UHPC.

In addition to different stresses at the interface surface, the thickness of the overlay has a significant influence on crack propagation. At thin overlay, partial delamination occurs at the interface due to the bending experienced by all sections of the repaired beam. In contrast, a 50 mm UHPC overlay provides sufficient stiffness, which resists bending. That caused delamination over a larger area of the beam's surface.

Future studies must deeply understand full bridge deck slab behavior under design loads.

REFERENCES

[1] Graybeal, B. (2011). Ultra-High Performance Concrete, *United States. Federal Highway Administration. Office of Infrastructure Research and Development*, No.FHWA-HRT-11-038.

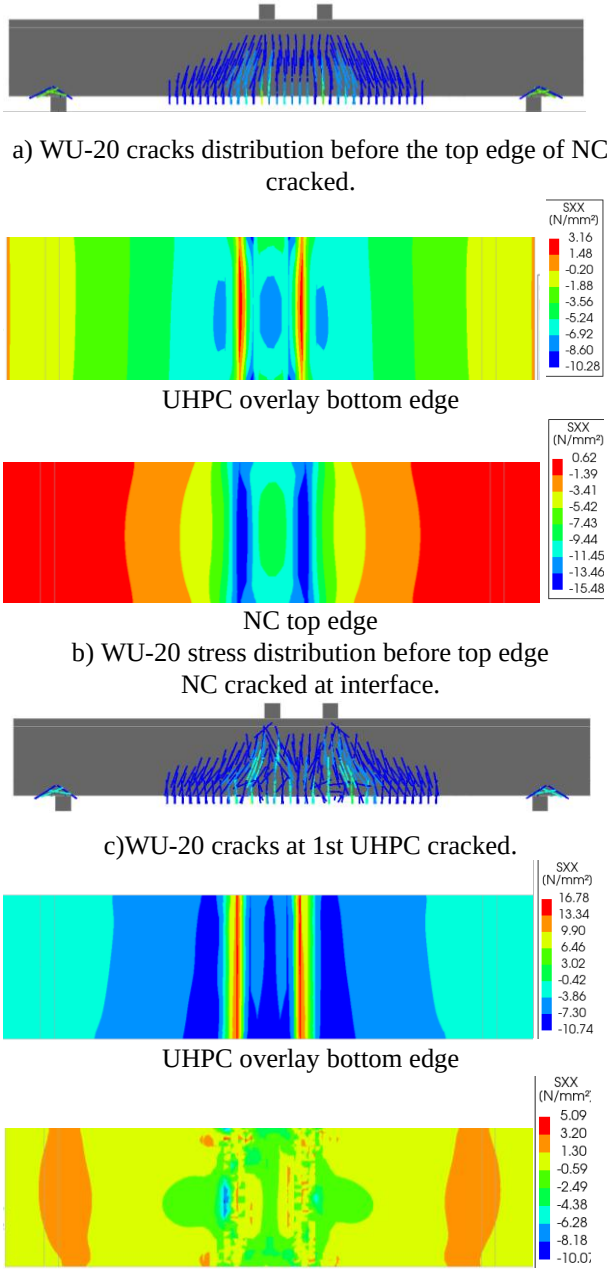

a) WU-20 cracks distribution before the top edge of NC cracked.

UHPC overlay bottom edge

NC top edge

b) WU-20 stress distribution before top edge NC cracked at interface.

c)WU-20 cracks at 1st UHPC cracked.

UHPC overlay bottom edge

NC top edge

d) WU-20 stress distribution at 1st UHPC cracked at interface

Figure 12: WU-20 FEM analysis before delamination.

[2] Wille K, Kim DJ, Naaman AE. Strain hardening UHP-FRC with low fibre contents. *Mater Struct 2011;44(3):583e98.*

[3] Mishra O, Singh SP. (2019) "An overview of microstructural and material properties of ultra-high-performance concrete". *J Sustain Cement-Based Mater;* **8**(2):97e143.

[4] J. Resplendino, 2004 First Recommendations for Ultra-High Performance Concretes and Examples of Application, *Proceeding of the International Symposium on Ultra High-Performance Concrete, University of Kassel, Kassel*, 79–90.

[5] Brühwiler, E., Bastien-Masse, M., Mühlberg, H., Houriet, B., Fleury, B., Cuennet, S., Schär, P., Boudry, F., Maurer, M., 2015. Strengthening the Chillon Viaduct Deck Slabs with Reinforced UHPFRC. *Proceedings 2015 IABSE Conference*, Geneva, Switzerland.

[6] Haber, Z. B., Munoz, J. F., & Graybeal, B. A., 2017. Field Testing of an Ultra-high Performance Concrete Overlay, *United States. Federal Highway Administration. Office of Infrastructure Research and Development*, No. FHWA-HRT-17-096.

[7] Hillerborg, A., Modeer, M., Petersson, P.E., 1976. Analysis of crack formation and crack growth in concrete by means of fracture mechanics and finite elements. *Cement and Concrete Research* **6**, 773–782.

[8] Willam, K., Pramono, E., Sture, S., 1987. Fundamental issues of smeared crack models. *SEM/RILEM International Conference on Fracture of Concrete and Rock, Houston, Texas*